Title

Imaging Mass Spectrometry Reveals Crosstalk between the Fallopian Tube and the Ovary that Drives Primary Metastasis of Ovarian Cancer

Journal

ACS Central Science, 4(10)

ISSN

2374-7943

Authors

Zink, Katherine E
Dean, Matthew
Burdette, Joanna E
et al.

Publication Date

2018-10-24

DOI

10.1021/acscentsci.8b00405

Peer reviewed

ACS central science

Research Article

Cite This: ACS Cent. Sci. 2018, 4, 1360−1370

http://pubs.acs.org/journal/acscii

Imaging Mass Spectrometry Reveals Crosstalk between the Fallopian Tube and the Ovary that Drives Primary Metastasis of Ovarian Cancer

Katherine E. Zink, Matthew Dean, Joanna E. Burdette, and Laura M. Sanchez*

Department of Medicinal Chemistry and Pharmacognosy, University of Illinois at Chicago, 833 South Wood Street, Chicago, Illinois 60612, United States

Supporting Information

ABSTRACT: High grade serous ovarian cancer (HGSOC) is the fifth leading cause of cancer deaths among women. New evidence suggests that HGSOC arises in the fallopian tube and then colonizes the ovary before spreading into the peritoneal space. Therefore, due to the proximity of this metastasis, an experimental design was optimized using imaging mass spectrometry to capture the spatial composition of small molecules uniquely expressed when fallopian-tube-derived tumor cells were grown in the microenvironment of the ovary as a model of primary metastasis. The observed mass-to-charge ratios (m/z's) that were induced specifically in coculture represent small molecules that may contribute to the metastasis of HGSOC selectively to the ovary. Human fallopian tube epithelial HGSOC and tumorigenic murine oviductal epithelial cells, but not normal cell types, repeatedly induced a signal from the ovary at m/z 170. This signal was identified as norepinephrine, which was confirmed to stimulate invasion of ovarian cancer cells lacking wild-type p53. These molecules may reveal pathways that contribute to metastasis and biological targets for therapeutic intervention to block ovarian metastasis of fallopian-tube-derived HGSOC. The developed mass spectrometry method can be adapted to other mammalian-based model systems for investigation of untargeted metabolomics that facilitate metastasis.

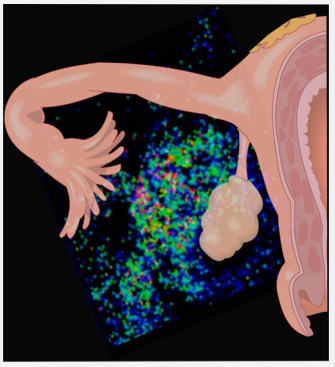

INTRODUCTION

Communication between a tumor and nearby normal cells influences many processes in early tumor development, such as chemoresistance, proliferation, and metastasis. This communication is poorly understood in high grade serous ovarian cancer (HGSOC) because recent evidence has shown that HGSOC begins in the fallopian tube, not the ovary.[1−9] The current model for the development and spread of fallopian-tube-epithelium-derived (FTE-derived) HGSOC is that normal FTE cells acquire changes such as loss of PAX2 and mutation of p53 resulting in stabilization of the protein (termed the p53 signature), that eventually form a serous tubal intraepithelial carcinoma (STIC).[10] STICs then metastasize to the ovary where a large tumor forms, resulting in what has been historically called ovarian cancer. The role of the reactive oxygen species (ROS) and proteins from the ovary in transformation of FTE cells and their migration to the ovary has recently been investigated.[11−14] A recent meta-analysis of metabolomic data produced from 11 studies across 7 different kinds of cancer showed widespread changes in metabolism of tumors relative to normal tissues.[15] These studies have largely focused on changes in metabolites as markers of altered cell metabolism, while the role of small molecules in cell-to-cell communication has been largely ignored. Small molecules have been linked to several disease states, and an innovative method is required for exploring factors that affect their secretion, determining their spatial resolution, and assessing their role in HGSOC metastasis.

Imaging mass spectrometry (IMS) is a technique whose applications are rapidly expanding, particularly for biological systems.[16] By merging an optical image of a given sample with the averaged mass spectrum of the sample's molecular components, IMS provides an untargeted metabolomics data set that enables researchers to select for a given mass-to-charge ratio (m/z) and visualize the spatial distribution of that particular m/z in an optical image of their sample. IMS has recently been a particularly powerful tool for microbial colony agar-based studies because the microbial colonies are visible to the naked eye, and a desiccated agar sample can easily be introduced into a time-of-flight (TOF) instrument.[17−22] Tissue imaging has also long captivated the focus of IMS investigators.[23−26] Recently, several papers have analyzed fresh frozen samples from ovarian cancer patients[27,28] and transgenic mouse models with FTE-derived ovarian cancer[29] using IMS. A 2D cell culture grown directly on glass slides has previously been analyzed using MALDI-TOF,[30] and 3D cell spheroids have been optimized to accurately represent the structure of certain mammalian tissues.[31] Both cell culture methods have been developed for analysis of human carcinomas, but only as 2D slices of fixed tissue samples. With human samples, tissue sections capture one static representation of a disease at a specific time point, usually at stage III or IV, when a tumor is compared with healthy tissue

Received: June 29, 2018
Published: October 9, 2018

DOI: 10.1021/acscentsci.8b00405
ACS Cent. Sci. 2018, 4, 1360−1370

to uncover relevant biomarkers. While these studies shed light on regulation or dysfunction in diseased tissue compared to a healthy sample, they have not yet been adapted to investigate the early dynamic chemical communication between different cells or tissues. Application of such a technique to the FTE and ovary, to understand the spatial distribution of chemical signals that govern ovarian colonization as the first step of FTE-derived serous tumor metastasis, could be valuable in uncovering the initial metabolic changes at this key step of disease progression. Thus, engineering a system where cellular models of cancer are incubated with organotypic ovaries would allow for a unique mechanism of studying biochemical signals between the fallopian tube and ovary. Such a system could be applied to multiple tumor types and different metastatic niches.

By designing an *in vitro* experimental setup that can capture the diffusible and dynamic chemistry between FTE-derived cells alongside a healthy ovary, it is possible to study chemical communication between cells. The focus of this study is between wild-type FTE cells and FTE cells engineered to represent various stages of transformation in ovarian cancer with healthy ovaries, modeling primary cellular communication during HGSOC metastasis to the ovary.[5] We hypothesize that diffusible small molecules are important mediators of exchange between the FTE-derived tumor cells and the ovary during metastasis. In this paper we present evidence that these early chemical signals can be captured by MALDI-TOF IMS using a 3D agarose-based mammalian cell culture and explant organ tissue, and we demonstrate the key role of one of these molecules, norepinephrine.

RESULTS

Elucidating early events in colonization of the ovary as the primary step in metastasis by FTE-derived HGSOC requires an understanding of chemical communication between the ovary and fallopian tube. To that end, a reproducible method for IMS analysis was developed to detect small molecular components (100−2000 Da) in an *in vitro* system that mimics this dynamic microenvironmental exchange (Figure 1). Initial studies to optimize the conditions for IMS were performed with MOE PTEN^{shRNA} cells, both because they are tumorigenic following xenograft[32] and so that the ovaries and FTE cells were from the same species, thus increasing the likelihood of dynamic communication between the ovary and FTE cells. The primary considerations for development of an IMS method to analyze spatial exchange of small molecules in coculture were that the sample was extremely flat and exhibited a spatial distinction between the MOE PTEN^{shRNA} cells and the healthy ovarian tissue, and that the ultimate layout included the greatest number of controls or treatments in a single experiment. We have outlined the optimization process for parameters that were critical to a successful IMS run in a MALDI-TOF instrument (see the Technical Optimization of the IMS Method section) and also to parameters that were required for biological accuracy (see the Optimization of HGSOC Representation section).

Technical Optimization of the IMS Method. *Optimal 3D Cell Culture Plating Was Achieved Using 300 μL of Material in an 8-Well Chamber and Resulted in Optimal Sample Height.* Compatibility with a time-of-flight (TOF) mass spectrometer requires a sample with a height of 0.4−1.0 mm. In general, agar-based samples used for microbial-based imaging are approximately 100−200 μm thick, and the agarose-based method was optimized to fall within this range

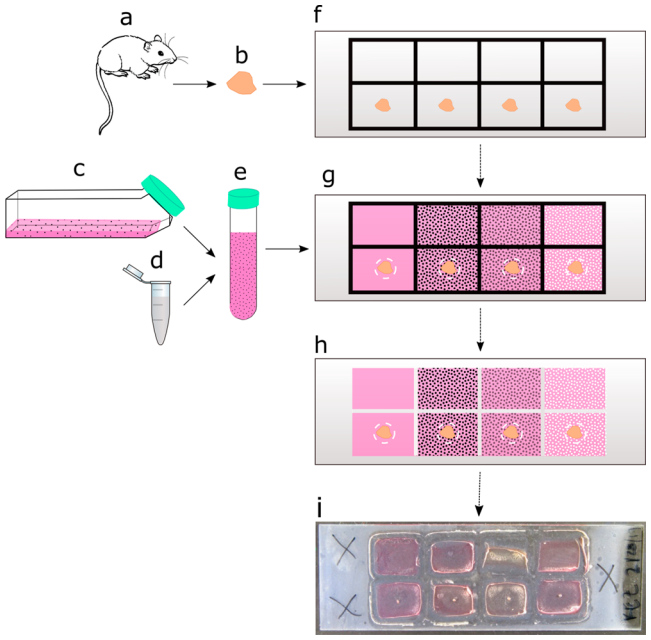

Figure 1. Optimized schematic for plating ovarian explants and MOE PTEN^{shRNA} cells in 3D coculture in agarose. (a) Female mice, aged 16−18 days, are sacrificed for ovary removal. (b) Explant ovarian tissues, termed explants, are maintained in warm media until plating. Ovaries are separated from the bursa and are halved just before plating. (c) MOE PTEN^{shRNA} cells are maintained in T-75 flasks in an incubator at 37°C. Cells are trypsinized and centrifuged into a pellet, and the spent media is aspirated. Cells are resuspended in a falcon tube in 1× DMEM media at a concentration of ∼333 cells/μL. (d) 2% low-melting agarose (in Eppendorf) is prepared, and 1 mL aliquots are liquefied on a hot plate at 70°C. (e) Cells suspended in 1× DMEM are mixed in a 1:1 ratio with 2% agarose, so the final concentrations are ∼166 cells/μL and 1% agarose. (f) Top view of the ITO-coated slide with an 8-well chamber adhered and centered to the glass. Ovarian explants are placed in the center of wells for coculture conditions. (g) 3D cell culture is plated in aliquots of 300 μL (approximately 50K cells) per well. Each cell type will have a "cell only" control well and a coculture well. White dotted lines indicate the position of the ovarian explant. (h) After 4 days of incubation at 37°C and 5% CO_2, the chamber is detached from the slide, leaving the 3D agarose plugs standing without contact to one another. The slide and agarose plugs are dried in a 37°C oven for 4 h, rotating 90° each hour. White dotted lines indicate the position of the ovarian explant. (i) Real slide after desiccation.

as well. Matrix application also increases the height of the sample but within the allowed height range with the use of the HTX TM sprayer.[21] The height of the sample is important because it can affect the mass calibration of the TOF instrument. This calibration depends on accurate timing; when a sample is irradiated at the surface at $t = 0$, analytes are simultaneously desorbed, and ions are separated in the time-of-flight tube toward the detector. A uniform sample height ensures that the distance traveled through the TOF tube is equal for all sample points, and thus the corresponding mass is accurate. The ovarian explant slightly alters the height of the sample, and the accompanying mass error can be calculated by utilizing the matrix peaks (Table S1).[33,34]

While the bacterial colony imaging procedure utilized agar,[21] the 3D cell culture was generated using agarose. Agarose allows for the diffusion of small molecules, while cells remain immobile. A layer of wet agarose approximately 2−3 mm dries to approximately 100−200 μm, ideal for accurate mass

DOI: 10.1021/acscentsci.8b00405
ACS Cent. Sci. 2018, 4, 1360−1370

analysis via MALDI-TOF.[21] Optimization of the amount of material and vessel for incubation required evaluation of several layouts. Cells were plated in different layering options (Figure S1), and 24-well plates, 6-well plates, and 8-well chamber slides were tested (Figure S2). For drying considerations, the 8-well chamber slide is optimal and requires only 300 μL of material (agarose, media, cells). The 8-well chamber also allows for plating, incubation, and desiccation to take place on the same slide. Over 4 h of desiccation in a 37 °C oven, the agarose plugs were thoroughly desiccated. During desiccation the slide was rotated 90° every hour to ensure even heat distribution and no agarose aggregation.

Matrix Was Applied in a Liquid Solution before Sample Plating and after Desiccation to Promote Adhesion of 3D Agarose Cultures to Glass Slides. Microbial IMS protocols have been optimized for application of a powdered matrix onto wet agar,[21] but attempted adaptation of this protocol to the agarose plugs determined that the moisture of the wet agarose plugs in our setup absorbed all the matrix and resulted in heterogeneous matrix cocrystallization and ion suppression (Figure S3). A matrix solution was therefore sprayed via airbrush (adapted from 17) onto a dried sample as opposed to sieved onto a wet sample. This solution was also used to prespray the plate to aid in adherence of the agarose plugs to the plate during incubation and desiccation. Airbrush application was later translated to spraying via a TM sprayer for more consistency across runs. This process was optimized using steel MALDI plates and subsequently adapted to glass slides. For the slides, approximately 5 mL of a 10 mg/mL solution (50:50 CHCA:DHB in 100% acetone) was sprayed as a precoat and 30 mL of the 10 mg/mL solution after agarose desiccation. The smaller crystal sizes resulting from sprayed matrix allowed for better spatial resolution (20−50 μm), compared with sieved matrix (100−200 μm), which was important considering the scale of the sample.

Cells Were Plated onto ITO-Coated Glass Slides Instead of Steel Plates To Facilitate Visual Verification of Homogeneous Cell Distribution Postdesiccation. The use of glass slides was necessary to validate microscopically the homogeneous distribution of the cells in each well, and to ensure that any detectable m/z signals were not simply the result of cellular aggregation or other factors. Agarose plugs were easily adaptable to glass slides, and cells were visibly homogeneous in the 3D suspension (Figure S4). Steel plates are not compatible with microscopic visualization, as they are not transparent. Commercial IMS data analysis software is not yet capable of overlaying signals with microscopic images, so verifying the distribution of cells before matrix application and subjection to laser irradiation allowed interpretation of the m/z signals detected based on location of tissue. An ITO-coated glass slide (ITO, indium tin oxide) was the ideal platform for plating because it allows for electric conductivity which improves the ionization and desorption of analytes in MALDI analyses compared to insulating surfaces, such as a standard glass slide.

Optimization of HGSOC Representation. *Cell culture of 166 Cells per μL Provided Ample Signal in IMS Data for Validation of Molecular Exchange.* As the initial approach was untargeted, it was unknown how dense of a cell culture was required to produce sufficient signal for detection in IMS. A homogeneous population of cells was necessary to distinguish cell types (e.g., ovarian vs fallopian tube vs media) from m/z's in media. Early cell density trials in 6-well plates optimized the cell density to be 166 cells per μL of material (Figure S5).

Eight-Well Chamber Slide Allowed Comparison of HGSOC Coculture to All Tissue, Media, and Cell Controls. Because the variability in sample preparation differs slightly for each IMS run, there can be no absolute comparison regarding molecular abundance between samples unless the data is acquired during the same experiment. The ability to include the greatest number of conditions and controls on one slide allows for direct comparison of abundance based on normalized intensities for each m/z. To circumvent the difficulty in cutting and transferring agarose plugs from other wells onto a glass slide, an 8-well divider from a chamber slide was placed directly on top of an ITO-coated slide, allowing agarose plating and incubation to be performed directly on the ITO slide (Figure S6). After 4 days of incubation, the chamber was detached from both the agarose plugs and the glass slide. This setup decreased the number of overall cells required for an experiment, allowed density verification via a microscope, required only a small amount of agarose (which dried quickly), and prevented the meniscus effect during drying. The final workflow adopted is shown in Figure 1.

Cells and Ovarian Tissue Designed with Spatial Distinction Revealed the Source of Molecular Exchange. The presence of one whole murine ovary versus $^1/_2$ of an ovary (hereafter termed ovarian explant) was tested. Evaluation of the resulting m/z's compared between a whole ovary and $^1/_2$ of an ovary suggested that molecular components produced by both tissues were consistent and comparable (Figure S7). Subsequent experiments therefore used ovarian explants consisting of $^1/_2$ of the ovary because these explants dried to an optimal height, and allowed us to responsibly maximize tissue obtained from animals.

Ovarian Explants Are Viable after 4 Days of Culture. Hematoxylin and eosin (H&E) staining of the ovarian explants after 4 days of culture in agarose showed a normal ovarian architecture, with ovarian follicles, stroma, and an intact ovarian surface epithelium (OSE) layer. Measuring ATP as a marker of viability showed that explants had a slightly lower average luminescence after 4 days of culture, but this did not reach statistical significance (Figure S8; $P = 0.22$, $n = 4$). These results indicate that ovarian tissue can survive and agrees with our previous results where ovarian explants were encased in an alginate bead and remained viable and intact for up to 8 days.[35,36] Confirming that cell lines could also survive for 4 days in agarose, MOE PTEN^{shRNA} red fluorescent protein (RFP) cells were clearly visible, with bright red fluorescence after 4 days of culture (Figure S8), which agrees with previous studies where cells were grown suspended in agarose for up to 4 weeks to access anchorage independent growth.[32]

MOE PTEN^{shRNA} Induced Unique Signals in an Ovarian Explant/FTE Coculture System. IMS was initially performed using four treatments (Figure S9): (1) agarose and media only (control), (2) MOE PTEN^{shRNA} cells, (3) an ovarian explant, and (4) both the ovarian explant and MOE PTEN^{shRNA} cells (coculture), all on a single slide. After 4 days of incubation, IMS was performed on a Bruker Autoflex speed LRF MALDI-TOF instrument at 50 μm resolution. Analysis of the resulting spectra using a statistical algorithm in SCiLS software (Bruker) detected 44 m/z's of interest that are statistically higher ($P < 0.05$) in the explant/MOE PTEN^{shRNA} coculture condition when compared to the average spectrum

DOI: 10.1021/acscentsci.8b00405
ACS Cent. Sci. 2018, 4, 1360−1370

from the regions of all four conditions (Figure S9 and Table S1).

IMS experiments were then designed to determine signals of the unique explant/MOE PTEN^{shRNA} coculture system when compared to normal cells. Murine ovarian surface epithelial (MOSE) cells were used as control to see if chemical signals were unique to fallopian tube cells or if a cell line derived from a different organ would trigger the same profile. In addition, MOE SCR^{shRNA} cells were used as a control to determine if the effect was elicited by all FTE cells or unique tumorigenic FTE cells. The experiment incorporated the following controls and conditions: (1) agarose and media only (control), (2) ovarian explant only in media, (3) MOE SCR^{shRNA} cells, (4) ovarian explant and MOE SCR^{shRNA} cells coculture, (5) MOE PTEN^{shRNA} cells, (6) ovarian explant and MOE PTEN^{shRNA} cells coculture, (7) MOSE cells, and (8) ovarian explant and MOSE cells coculture (Figure 2). Mass error was calculated for each run, and all identified signals were adjusted postacquisition to incorporate the mass shifts based on matrix peaks (Table S2). According to the imaging software SCiLS (version 2015b), 33 m/z signals were significantly increased ($P < 0.05$)

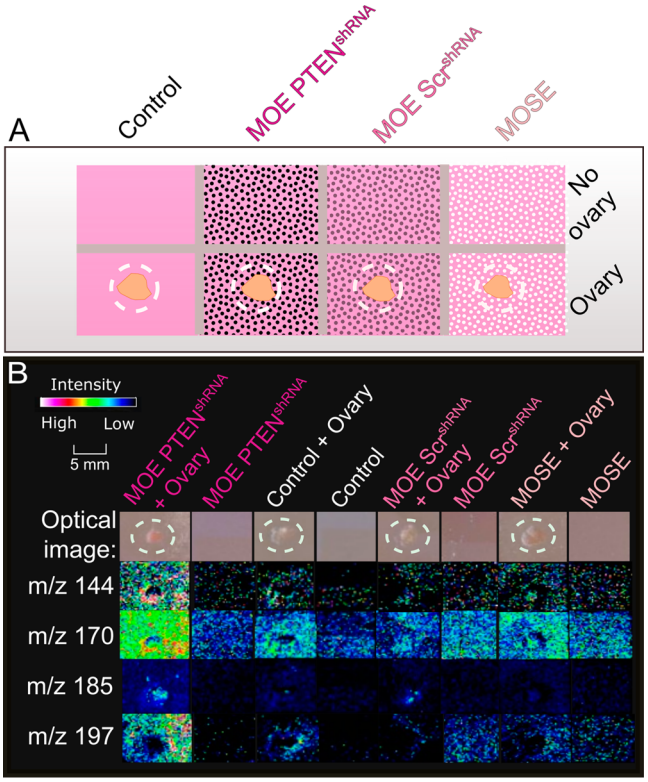

Figure 2. IMS method developed was thoroughly compatible with a MALDI-TOF instrument and ensured biological specificity. Ovaries are indicated by a surrounding dotted white circle. (A) Illustration of the optimized slide layout. MOE SCR^{shRNA} is the WT murine oviductal epithelial cell line and is used to ensure that any m/z signals detected in the HGSOC condition is specific to the PTEN mutation. MOSE is the murine ovarian surface epithelium cell line, which serves as a control to verify that signals are specific to the MOE cell line. All agarose plugs are 300 μL in volume, and 1% agarose. (B) Four m/z signals that displayed significant differences in regulation in the well with half of an ovary embedded in MOE PTEN^{shRNA} cells. The m/z's of 144, 170, 185, and 197 are produced in statistically higher abundance ($p < 0.05$) in the MOE PTEN^{shRNA}/ovary coculture, indicating they are the result of interaction.

(Figure S10 and Table S1). Figure 2 illustrates four representative m/z's from the IMS analysis that occur in the explant/MOE PTEN^{shRNA} coculture ($n = 3$). The combination of explant/MOE PTEN^{shRNA} elicited a strong increase in signal at m/z 170 (Figure S11 shows MS^1 spectra of a representative IMS run).

One of the signals detected in both IMS runs, m/z 170, was putatively matched in the Human Metabolome Database (HMDB) to norepinephrine, based on the protonated norepinephrine mass of 170.08 (Figure 3).[37] HMDB was used to search possible matching compounds from the nominal mass of m/z 170 because search results in this particular database include compounds that are relevant to a mammalian tissue coculture model such as that assessed in this study. While most of the mass signals from Figures S9 and S10 were searched in HMDB, there is already an evidenced collection of literature that shows that the ovary can produce norepinephrine in other contexts and implicates norepinephrine as an influential molecule in ovarian cancer, and therefore m/z 170 became the priority molecule for elucidation. Further dereplication is done following identification of high-resolution mass.

Ovarian Explant/FTE Coculture Significantly Upregulates Production of Norepinephrine. The m/z 170, putatively norepinephrine, was chosen for further investigation because norepinephrine has been documented to stimulate invasion, migration, and chemotherapy resistance in ovarian cancer[38−42] cells. Long-term use of antagonists of adrenergic receptors (i.e., beta blockers) is associated with longer overall survival in ovarian cancer patients.[43] To validate that this IMS method was accurately detecting real and relevant small molecules, a standard of norepinephrine was purchased (L-(−)-norepinephrine-(+)-bitartrate, EMD Millipore Corp., Billerica, MA). Norepinephrine ([M] = $C_8H_{11}NO_3$) has an exact mass of 169.0739 g/mol, and a calculated exact mass after protonation of m/z 170.0817 ($[M + H]^+$). Norepinephrine was detected in positive mode on an Agilent 6550 iFunnel Q-TOF instrument via direct infusion in the standard at m/z 170.0810 (4.11 ppm error) and the coculture extract at m/z 170.0818 (0.58 ppm error) (Figure S12). With a high-resolution mass acquired, a second LC-MS search was performed in HMDB, searching for compounds with $[M + H]^+ = m/z$ 170.0818 to validate that the mass from the extract sample matched that of norepinephrine. A search of the proposed chemical formula and experimental protonated mass independently showed six possible matching compounds, one being norepinephrine (Table S3). Two configurations of norepinephrine are included in the table, and, interestingly, two other compounds (5- and 6-hydroxydopamine) are in the norepinephrine biosynthesis pathway.

In positive mode, the pure standard is characterized most prominently by the major in-source fragment at m/z 152.0703 ($[M - H_2O + H]^+$, calculated for $C_8H_{10}NO_2^+$), which represents the loss of water from the structure (Figure 3). MS/MS fragmentations of both the standard and extract sample were analyzed via direct injection, due to lack of retention under standard LC conditions (data not shown). Direct injection of the extracted sample indicated the presence of both the intact norepinephrine molecule as well as the major fragment $[M - H_2O + H]^+$. The structure of norepinephrine is shown in Figure 3A. Figure 3B displays the MS/MS spectra of both standard and coculture extract with a precursor ion of m/z 152.0705 and m/z 152.0707 in the MS^1, respectively (Figure

DOI: 10.1021/acscentsci.8b00405
ACS Cent. Sci. 2018, 4, 1360−1370

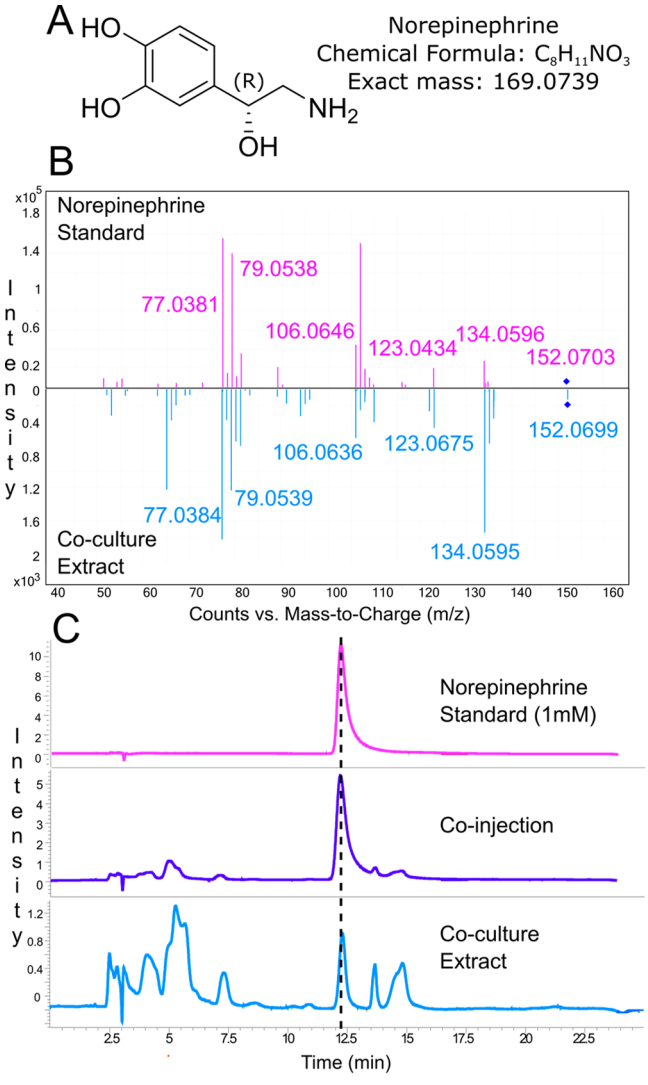

Figure 3. Analysis of coculture extracts and comparison to standards detected norepinephrine is produced in explant/MOE PTEN^{shRNA} coculture. (A) Structure of norepinephrine. (B) On an Agilent 6550 iFunnel Q-TOF instrument, the precursor ions of m/z 152.0703 in the norepinephrine standard and m/z 152.0699 in the explant/MOE PTEN^{shRNA} coculture extract were fragmented using a collision energy of 25 eV and an isolation window of 1.3 amu. Tandem MS/MS of the norepinephrine standard and the extract introduced via direct injection elucidated five ESI fragments shared between the norepinephrine standard and the coculture extract. (C) HPLC-UV chromatograms on a HILIC column under aqueous normal phase HPLC conditions [A = 30 mM ammonium acetate (pH = 4), B = ACN + 0.02% FA, 5−15% A over 20 min, 1 mL/min] were detected using a diode-array detector (DAD). HPLC traces in C are detected at 270 nm by a UV system, and additional wavelengths are shown in Figure S14. The retention time of the norepinephrine standard at 12.2 min (1 mM, top) matched a peak from the coculture extract at 12.3 min (bottom). When the two samples were coinjected (middle), the peak seen in the NE standard chromatogram grew larger at 12.2 min and maintained the same retention time, indicating norepinephrine is present in all samples.

S12). There is a slight difference in reported $[M - H_2O + H]^+$ between the MS^1 experiment (Figure S12) and the reported precursor mass in Figure 3B because at the chosen isolation window and collision energy, the precursor mass has been depleted in the tandem mass spectrometry experiment. Five matching MS/MS fragments were clearly detectable in both samples. Differences in detected m/z values can be found in Table S4. HMDB contains MS/MS spectra of all six structures with the same chemical formula and mass, and while none matched perfectly to the experimental data, at least one other compound was eliminated as being m/z 170. Although the extracted coculture sample does not contain the standard's base peak at m/z 107, differences in ion abundance can result in differences in the corresponding MS/MS peaks. Given the low sample concentration of the coculture serving as a proxy for abundance when compared to the commercial standard, further analytical experiments were performed to definitively identify norepinephrine.

Because the fragmentation data still did not entirely identify norepinephrine as the compound of interest and because the instrument used for MS/MS fragmentation was not configured for polar analyte retention, an orthogonal method of analytical chemical dereplication was required. Using HPLC retention time and UV profiles as an orthogonal method of confirmation, a chromatographic method was developed under normal aqueous phase conditions on a HILIC (hydrophilic interaction liquid chromatography) column to retain the extremely polar norepinephrine long enough for valid confirmation of retention times. Under these conditions [A = 30 mM ammonium acetate (pH = 4), B = ACN + 0.02% FA, 5−15% A over 20 min, 1 mL/min], the norepinephrine standard alone eluted at 12.2 min; the extract alone eluted norepinephrine at 12.3 min, and the coinjection eluted norepinephrine at 12.2 min (Figure 3C), thus confirming our assignment as norepinephrine. Minor differences in retention time are within error, considering the complexity of the extract. UV databases identify only one UV maximum (λ_{max}) at 280 nm for norepinephrine. The matching UV profiles for the standard, coculture extract, and coinjection can be found in Figure S13, all with λ_{max} = 281 nm. Of the six compounds in Table S3, only norepinephrine has a UV profile that matches that detected in the coculture extract, therefore eliminating all other compounds from Table S3 as the compound of interest. Four wavelengths were utilized for the detection of norepinephrine on the orthogonal HPLC instrument, and all wavelengths agreed that no other peaks eluted at the same retention time (RT) as norepinephrine, indicating that it eluted independently and therefore could not be a compound other than norepinephrine (Figure S14).

Very little norepinephrine was detected in wells containing MOSE or MOE SCR^{shRNA} cells or in wells containing ovarian explant/MOSE or ovarian explant/MOE SCR^{shRNA}, indicating that the norepinephrine secretion is unique to tumorigenic cells incubated in the ovarian microenvironment.

MOE PTEN^{shRNA} Induced Signal Originates from the Ovary. Due to high abundance of m/z signals in the ovarian explant/MOE PTEN^{shRNA} condition and the placement of the ovary directly with the cells, it proved difficult to determine whether the ovary or the MOE PTEN^{shRNA} cells were the origin of the norepinephrine signal. Therefore, a setup was established where the murine explant was plated in agarose on one side of the well, and the MOE PTEN^{shRNA} cells were isolated to the opposite side (Figure S15). After 4 days of incubation, the slides were imaged under the same parameters as before. Nine signals were observed with the statistical software that replicated the initial experiments and demonstrated that the ovarian explant was the source of most of the signals (Figure S16). Visual examination of the divided

DOI: 10.1021/acscentsci.8b00405
ACS Cent. Sci. 2018, 4, 1360−1370

chambers indicates that m/z 170 is produced by the ovary and secreted into the agarose in the direction of the cell culture (Figure 4). In agreement, the ovary has been shown to produce and store norepinephrine,[44,45] with highest abundance just before ovulation.[46,47] Norepinephrine production was undetectable in ovarian cancer cells.[48] While the ovary contains sympathetic innervation, the granulosa cells also express catechol-*O*-methyltransferase (COMT), monoamine oxidase A, and the NE transporter.[49,50]

Norepinephrine Stimulates Invasion of Cells that Lack Wild-Type p53. Norepinephrine has repeatedly been shown to stimulate invasion of SKOV3 ovarian cancer cells and to increase metastasis *in vivo*.[38,42] Therefore, norepinephrine was tested to determine if it stimulated invasion of SKOV3 cells through Matrigel. As expected, norepinephrine (10 μM) stimulated invasion 2.2-fold over control ($P < 0.01$; Figure 5A). Based on genetic sequencing studies, SKOV3 are unlikely to have originated from the FTE.[1,51] Therefore, the ability of norepinephrine to stimulate invasion of human fallopian tube cells engineered to be tumorigenic due to SV40 and c-myc expression (FT33 Myc) was tested. In these cells, norepinephrine stimulated invasion 2.6-fold ($P < 0.01$; Figure 5B), indicating norepinephrine stimulates invasion of FTE-derived ovarian cancer cells. Norepinephrine had no effect on invasion of MOE SCR^{shRNA} or MOE PTEN^{shRNA} cells (Figure 5C,D). SKOV3 cells are p53 null; FT33 myc express SV40 (making them functionally p53 null), and p53 is mutated in 96−100% of HGSOC patients.[52] Furthermore, mutant p53 has been linked to migration and invasion of ovarian cancer cells.[53,54] Therefore, the ability of norepinephrine to stimulate invasion was tested in the presence of p53^{R273H}, the most common p53 mutation in HGSOC.[52] Norepinephrine increased invasion of both MOE p53^{R273H} and MOE p53^{R273H} + PTEN^{shRNA} cells approximately 2-fold ($P < 0.05$; Figure 5E,F), confirming a role for mutant p53 in norepinephrine-stimulated invasion of FTE-derived HGSOC cells.

DISCUSSION

Communication between adjacent cells and tissues is a key aspect of both normal and tumor processes. Transcriptomic and proteomic studies have highlighted the role of proteins in mediating signals that stimulate proliferation, metastasis, and chemoresistance of tumor cells.[55,56] However, recent metabolomic studies have shown widespread changes in metabolism within tumors and tumor cells,[57] and raise the possibility that secreted small molecules also mediate cell-to-cell communication within the tumor microenvironment. To that end, we developed an IMS procedure that can capture the dynamic communication between tissues and cells. Here, we used this procedure to understand how communication between the ovary and FTE changes during transformation of normal FTE to HGSOC. Importantly, this procedure could be adapted to study communication between multiple cell or tissues types.

Several research groups have developed IMS methods that map the molecular composition of mammalian tissues and cells, but primarily as individual tissue types. Beyond spheroids, little exploration has been done toward developing a protocol for 3D mammalian cell culture in agarose for imaging by MALDI-TOF mass spectrometry. Spheroids are also limited to analysis of cell lines that can form structured architecture, and the isolated growth conditions are not always amenable to cell coculture with tissues or organs. Desorption electrospray ionization (DESI) had been used to analyze differences in lipid

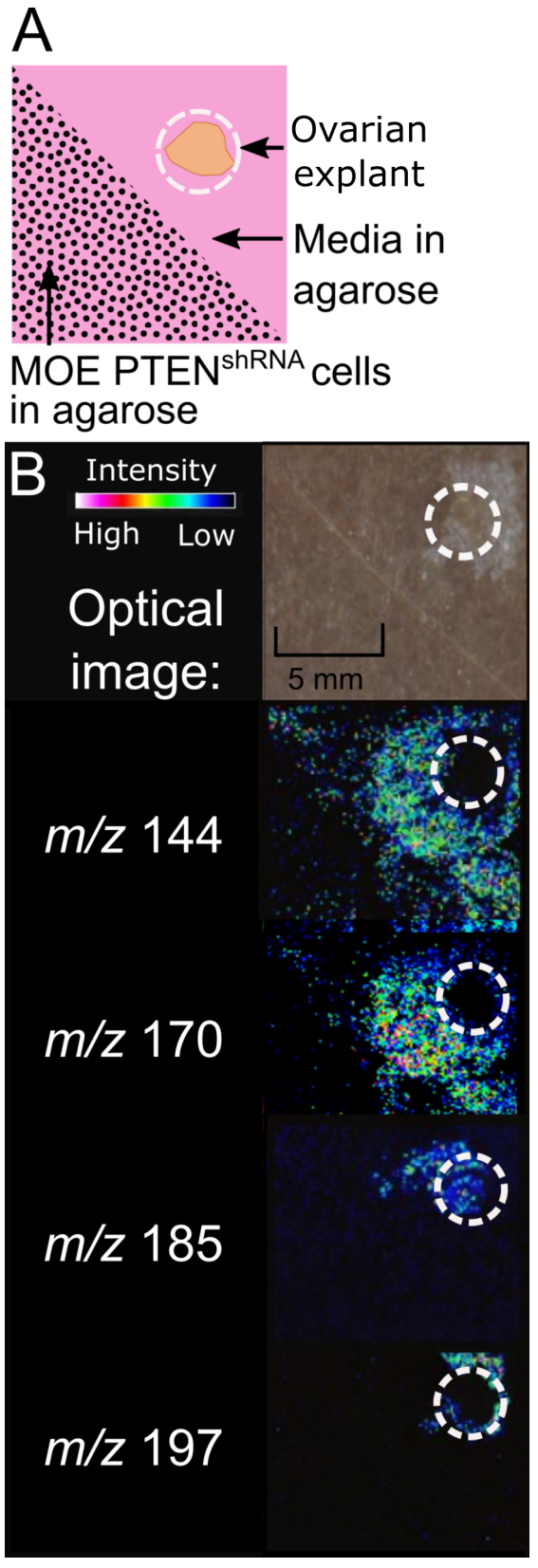

Figure 4. Signals in a divided well layout were replicated. (A) Cartoon illustration of the divided well setup designed to determine the origin of the signals produced when an ovary is incubated in MOE PTEN^{shRNA} cell culture. Cells were plated in DMEM media at a concentration of 166 cells/μL on one-half of the chamber, divided with a plastic tab. Once set, the plastic tab was removed, and DMEM alone in agarose was plated in the other half of the chamber. One half

DOI: 10.1021/acscentsci.8b00405
ACS Cent. Sci. 2018, 4, 1360−1370

Figure 4. continued

ovary was embedded into the media without contact with the cells. (B) All signals represented in Figure 2 are replicated when cells and ovary are physically separated in agarose. All signals here, including m/z 170, originate from the ovarian tissue.

composition in negative mode across the tumorigenic region of the reproductive system.[29] While many lipid species have been detected and assigned to healthy vs tumor sections, DESI is a matrix-free approach and therefore is targeted to best detect lipids when negative mode is employed. Lipids are important molecules in many disease pathways, but small molecules outside of the lipid classes continue to be underexplored. MALDI, converse to DESI, can utilize several matrices to enhance ionization of different chemical classes, and different matrices are available for either positive or negative mode analyses. The only requirement for detection is that the molecule is ionizable via MALDI. The initial analyses of the ovarian and fallopian tube microenvironments were focused on the small molecules being exchanged, and we have specifically optimized our experiments for detection of small molecules in positive reflectron mode. As our novel method combines the untargeted detection with a concentrated 2D representation of a 3D system, this platform provides a valuable opportunity to visualize how tissues and cells interact with one another through space as well as within their own cell types. In the case of HGSOC, the spatial exchange between the FTE and ovary characterizes a crucial stage of progression, and the IMS method described here can be used to interpret this chemical communication. Unique to this IMS setup, the agarose plugs of tissue and cells are dried from a 3D to a 2D structure that maintains all of the exchanged chemistry, not sectioned like other tissue approaches to IMS. This approach provides comprehensive analysis of the entire 3D environment, as opposed to tissue sections that are only selective of one representative layer of tissue.

Previous studies using IMS to study ovarian cancer have focused on tissue sections from transgenic mice[29] or ovarian cancer patients.[27,28] These studies have compared normal to diseased tissue or analyzed differences between different histotypes of ovarian cancer. In contrast, the current investigation focused on communication between the FTE (as an origin of HGSOC) and the normal ovary in an attempt to characterize interactions between these two tissues. We detected signals that were increased (e.g., m/z's 144 and 170) in coculture of tumorigenic FTE cells with normal ovaries. These changes were not seen in coculture of normal cells with the ovary, or in wells with ovaries or tumorigenic cells by themselves, suggesting that transformation of the FTE dramatically changes the chemistry between the FTE and the ovary. We also detected signals altered by transformation of the cells, regardless of whether an ovary was present, such as the increase of m/z 185, which likely reflects the altered metabolism due to loss of PTEN. Future work is needed to identify these signals and characterize their biological role in metastasis.

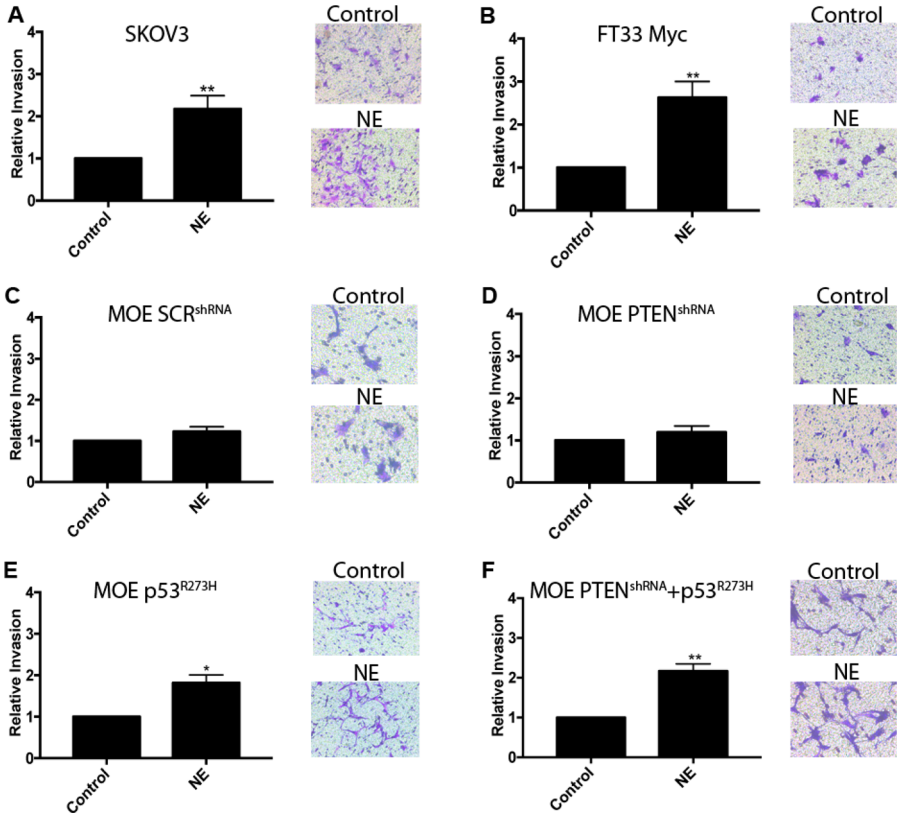

Figure 5. Norepinephrine (NE) stimulates invasion of HGSOC and FTE cells that lack functioning p53. (A, B) NE stimulates invasion of both SKOV3 and FT33-Myc, which are derived from the fallopian tube and express Myc and SV40 (making them functionally p53 null). (C, D) NE does not affect invasion of MOE SCR^{shRNA} or MOE PTEN^{shRNA} cells. NE stimulates invasion of MOE cells that stably express p53^{R273H} alone (E) or p53^{R273H} combined with PTEN^{shRNA} (F).

DOI: 10.1021/acscentsci.8b00405
ACS Cent. Sci. 2018, 4, 1360−1370

Using our newly developed IMS procedure, we visualized that coculture of murine ovaries with MOE PTEN^{shRNA} resulted in a dramatic increase in norepinephrine secretion from the ovary. Dereplication from the initial mass signal to identification as norepinephrine required rounds of elimination of other biologically feasible compounds with matching accurate masses. A collection of fragmentation patterns, exact experimental mass, UV profiles, and retention time matching verified the identification of norepinephrine in the explant/MOE PTEN^{shRNA} extract. It is well established that the ovary can produce and secrete norepinephrine in response to stress. However, this is the first report to show that tumor cells can alter the secretion of the ovarian NE. The role of norepinephrine in ovarian cancer progression is well established. In ovarian cancer patients, use of beta blockers has been associated with longer survival.[43,48] Functionally, norepinephrine has been repeatedly shown to stimulate invasion of ovarian cancer cells.[38,48] Armaiz-Pena et al.[48] found that norepinephrine activated Src through beta adrenergic receptors and protein kinase A. More recently, Nagaraja et al.[58] found that norepinephrine stimulated *INHBA* expression in ovarian cancer cells, which then recruited cancer associated fibroblasts (CAFs). Interestingly, norepinephrine stimulated invasion of SKOV3, FT33 Myc, MOE p53^{R273H}, and MOE PTEN^{shRNA} + p53^{R273H} cells but did not stimulate migration of MOE SCR^{shRNA} or MOE PTEN^{shRNA} cells. Therefore the loss of normal p53 signaling contributing to norepinephrine-stimulated invasion. A p53 mutation is known to increase migration and invasion of many cell types, which agrees with our data. Specifically, expression of p53^{R273H} is known to increase migration of MOE cells when using FBS as the chemoattractant.[54,59] However, this is the first time that mutation in p53 has been linked to norepinephrine-stimulated invasion of ovarian cancer cells.

To conclude, using an innovative IMS procedure, the current work shows that FTE-derived cancer cells, but not normal cells, can stimulate the release of norepinephrine from the ovary. Given the chemotaxic effect of norepinephrine, this secretion likely contributes to migration of tumor cells from the fallopian tube to the ovary, a key step in HGSOC progression. These results highlight the utility of IMS in studying chemical communication between tissues and cells in a 3D context that better recapitulate *in vivo* interactions. This approach has the potential to be applied to a vast range of cell and tissue types to address many conditions. With our initial findings, the elucidation of other detected *m/z*'s will be the immediate future research focus, and the construction of biological pathways leading to metastasis will also be a priority in the study of HGSOC.

METHODS

Mouse Colony and Ovary Removal. CD-1 mice were obtained from in-house breeding. Animals were housed in a temperature and light (12L:12D) controlled environment. Water and food were provided *ad libitum*. All animals were treated in accordance with the National Institutes of Health Guide for the Care and use of Laboratory Animals. Day 16−18 after birth ovaries were removed, dissected free of the uterus, fallopian tube, and bursa using a dissecting microscope (Leica MZ6, Buffalo Grove, IL).

Cell Lines. Spontaneously immortalized murine oviductal epithelial (MOE, equivalent of human FTE) cells and murine ovarian surface epithelial (MOSE) cells were graciously donated by Dr. Barbara Vanderhyden, U. of Ottawa. MOE cells stably expressing a scrambled control shRNA (SCR^{shRNA}), an shRNA targeting the gene PTEN (PTEN^{shRNA}), or overexpressing the R273H mutation in p53 (p53^{R273H}) had been previously generated and described.[32,54] FT33 Myc cells are a human fallopian tube secretory epithelial cell line transformed with SV40 and c-Myc[60] and were generously donated by Ron Drapkin, University of Pennsylvania.

Cell Culture. MOE cells were maintained in αMEM (10-022-CV, Cellgro, Manassas, VA) supplemented with 10% FBS (FB5001, Denville Scientific, Holliston, MA), 2 mM L-glutamine (30005068, CellGro, Manassas, VA), 10 mg/mL ITS (11074547001, Roche, Indianapolis, IN), 1.8 ng/mL EGF (100-15, Peprotech Inc., Rocky Hill, NJ), 100 U/mL penicillin−streptomycin (15140-122, Gibco, Grand Island, NY), 1 mg/mL gentamycin (30-005-CR, CellGro, Manassas, VA), and 18.2 ng/mL estradiol-17β (E1024-1G, Sigma-Aldrich, St. Louis, MO). MOE SCR^{shRNA}, PTEN^{shRNA}, and p53^{R273H} were maintained in similar media but with selection antibiotic. MOSE cells were maintained in media similar to MOE cells except estradiol was not added. FT33 Myc cells were maintained in DMEM/F-12 media (11330-032, Thermo Scientific, Waltham, MA) supplemented with 2% Ultroser G serum substitute (15950-01, Pall Corporation, Port Washington, New York). SKOV3 cells were maintained in McCoy's 5A (LT 16600-082, Life Technologies) supplemented with 1.1 g of sodium bicarbonate per 500 mL, and 10% FBS. Cells were passaged every 3−4 days and incubated at 5% CO_2 and 37 °C.

Invasion Assay. Matrigel (356234, Corning) was diluted to 300 μg/mL in αMEM media (10-022-CV, Gibco). Then 120 μL of diluted Matrigel was added to each Boyden chamber insert with 8 μm pores (PI8P01250, Millipore) and incubated for 1 h at 37 °C. Each cell line was collected with trypsin, counted, centrifuged, and resuspended in αMEM. Each cell line (50 000 cells per insert) was added to the top of each insert. αMEM (500 μL) with either 0.1% DMSO (vehicle control) or 10 μM norepinephrine dissolved in DMSO was placed under each Boyden chamber and used as the chemoattractant. After 24 h, the Matrigel and noninvaded cells remaining on top of the inset were removed with a cotton swab. Cells that invaded through the Matrigel and were on the bottom of the inset were fixed with paraformaldehyde, permeabilized with 70% methanol, and stained with crystal violet. Images of stained cells were captured with an inverted microscope and counted with ImageJ.

Seeding Cells into Agarose. The 2% agarose was liquefied at 70 °C. Cells in 10 mL of αMEM media maintained in T-75 flasks were washed with 10 mL of PBS and collected with 1 mL of 1× trypsin. Trypsinized cells were collected in 10 mL of αMEM, counted with a hemocytometer, and then centrifuged for 5 min at 800 rpm (Eppendorf 5810R). After aspiration of the αMEM media, cells were resuspended in 2× DMEM supplemented with 10% FBS and 2× penicillin−streptomycin (Sigma D5030-10L) to a concentration of 333 cells/μL. Cell suspensions were mixed with an equal amount of 2% agarose to produce a final cell concentration of 166 cells/μL in 1% agarose.

Slide Preparation and Plating. An 8-well Permanox chamber slide (Lab-Tek 177445) was attached to an ITO-coated microscope slide, which allowed for up to eight different conditions to be plated on a single slide. Cell lines or ovaries were seeded into each well as described in the results.

DOI: 10.1021/acscentsci.8b00405
ACS Cent. Sci. 2018, 4, 1360−1370

Incubation and Drying. Chamber slides with agarose plugs were incubated with a lid in 5% CO_2 and at 37 °C for 4 days. The 8-well chamber was detached from the slide prior to desiccation. Slides were dried in a 37 °C oven for 4 h, rotating 90° every hour.

Matrix Application. Spraying application was adapted from a protocol designed for matrix application to microbial colonies.[17] A 50:50 mixture of α-cyano-4-hydroxycinnamic acid (CHCA (98%), Sigma) and 2,5-dihydroxybenzoic acid (DHB (98%), Sigma) was recrystallized in-house. [Procedure: Dissolve the CHCA in warm ethanol, filter and add two volumes of deionized water. Let the solution stand overnight in the refrigerator, and filter the light yellow solid. Dissolve the compound in hot deionized water, and filter the hot solution through a fritted glass filter. Collect the crystals by filtration and dry under air and then on a high vac to obtain buff-colored crystals.) Recrystallized 50:50 CHCA:DHB was dissolved in 100% acetone at 10 mg/mL. Matrix was applied with an airbrush (Veda WD-180) using N_2 as a carrying gas at 30 psi. Approximately 300 mg of the matrix solution was sprayed across the slide of agarose in a horizontal manner with no drying time. Optimized experiments utilized a TM sprayer for matrix application, using a 50:50 CHCA:DHB mixture dissolved in 90:10 ACN:H_2O, and 0.1% TFA. Proper matrix application results in comprehensive sample coverage and a dull agarose appearance.

MALDI-TOF Analysis. Prior to IMS analysis, slides were scanned at 1200 dpi, and resulting images were used to guide irradiation. Imaging mass spectrometry data was acquired using flexControl v 3.4 at 50 μm spatial resolution on an Autoflex Speed LRF instrument (Bruker Daltonics, Billerica, MA) over the mass range 100−2000 Da. In positive reflectron mode, laser power was set to 40%, laser width to 2 (small), and reflector gain to 2.0×. For each raster point 500 laser shots at 2000 Hz were shot in a random walk method. Data was subsequently analyzed in flexImaging v 4.1 × 64 (Bruker Daltonics, Billerica, MA, USA). All spectra were normalized to the total ion count (TIC). The instrument was calibrated manually using phosphorus red.

Ovarian Explant Tissue Architecture and Viability. Ovarian explants were embedded in agarose in an 8-well slide as described above and incubated for 4 days. Explants were then removed from agarose, fixed overnight in 4% paraformaldehyde, dehydrated, and embedded in paraffin. Explants were sectioned (5 μm), deparaffinized with xylene, rehydrated, and stained with hematoxylin and eosin (H&E). Images were captured at 10× and 40× with a Nikon Eclipse E600 microscope. To quantify explant survival over the 4 day incubation, viability was measured with the CellTiter-Glo 3D cell viability assay (G9681, Promega). Explants were removed from agarose on days 0 and 4, and incubated in 100 μL of CellTiter-Glo reagent for 15 min. Luminescence was measured with a Syngergy Mx BioTek plate reader. To confirm that cell lines could survive in agarose for 4 days, MOE $PTEN^{shRNA}$ cells stably expressing red fluorescent protein (RFP) were embedded in agarose and imaged after 4 days.

Statistical Analysis. SCiLS software (Bruker, version 2015b) was used to verify statistical significance in molecular abundance. All data was normalized to the TIC, and the colocalization algorithm was employed to detect m/z's specific to the region of interest. For statistical significance the Pearson correlation coefficient was set to $P < 0.05$, and no denoising was performed. Significant signals were exported as images in flexImaging for figure generation. For invasion and viability experiments, data was analyzed with t tests using Prism (version 7.0a).

Extraction and Dereplication. Agarose plugs of MOE $PTEN^{shRNA}$ cells incubated with ovarian explant were plated and incubated as detailed above. After, the agarose plugs were collected in a 4 mL vial and extracted in 1 mL of ACN. The ACN extraction was sonicated for 1 h and centrifuged at 10K rpm for 2 min. Dereplication and prioritization of m/z signals were done using the Human Metabolome Database (HMDB) to generate a candidate list of compounds based on nominal masses followed by literature searching the role these molecules have been documented to have in cancer.

MS/MS Analysis. MS/MS analysis was performed on an Agilent LC 1290 instrument interfaced to an Agilent 6550 iFunnel Q-TOF device. The coculture extract and the standard [100.00% pure norepinephrine standard (L-(−)-norepinephrine-(+)-bitartrate, EMD Millipore Corp., Billerica, MA)] were prepared in 90:10 ACN:H_2O with 0.1% TFA to 10 μg/mL. Samples were analyzed by direct infusion with a collision energy of 25% and an isolation width of 1.3 amu.

HPLC Analysis. The norepinephrine standard and the coculture extract were analyzed on an Agilent 1200 series instrument equipped with a DAD for retention time matching. Under aqueous normal phase conditions, 10 μL of (1) a 1 mM norepinephrine standard, (2) the coculture extract, and (3) an equal mixture of the two were injected onto a Luna 5 μm HILIC column (150 × 4.60 mm; Phenomenex), with a security guard (Phenomenex). Solvent A was 30 mM ammonium acetate, pH = 4, and solvent B was ACN + 0.02% FA. The gradient was 5−15% A over 20 min, at 1 mL/min. UV monitoring was performed at 210, 250, 254, and 270 nm.

Safety. No unexpected or unusually high safety hazards were encountered in this line of research.

Data Repository. All IMS data referenced in this article can be found in the MassIVE Database under ID MSV000082401. LC-MS/MS data on norepinephrine and extracts can be found on MassIVE under ID MSV000081960.

■ ASSOCIATED CONTENT

Supporting Information

The Supporting Information is available free of charge on the ACS Publications website at DOI: 10.1021/acscentsci.8b00405.

> Additional information regarding sample preparation optimization including embedding, drying, matrix application, target plates, cell density, and ovary preparation; cell and ovary viability; IMS and statistical analysis for signals not discussed in the main text; and MS/MS analysis of standard vs extract and ppm errors (PDF)

■ AUTHOR INFORMATION

Corresponding Author

*E-mail: sanchelm@uic.edu. Phone: (312) 996-0842.

ORCID

Laura M. Sanchez: 0000-0001-9223-7977

Notes

The authors declare no competing financial interest.

DOI: 10.1021/acscentsci.8b00405
ACS Cent. Sci. 2018, 4, 1360−1370

■ ACKNOWLEDGMENTS

We thank Drs. Atul Jain and Terry Moore for assisting with the recrystallization of the MALDI matrices. Funding was provided by the Chicago Biomedical Consortium with support from the Searle Funds at The Chicago Community Trust (C-076) (L.M.S.); Grant K12HD055892 from the National Institute of Child Health and Human Development (NICHD) and the National Institutes of Health Office of Research on Women's Health (ORWH) (L.M.S.); University of Illinois at Chicago Startup Funds (L.M.S.); T32 AT007533 from NCCIH and Grant 543296 from the Ovarian Cancer Research Fund Alliance (M.D.); and UG3 ES029073 (J.E.B.).

■ REFERENCES

(1) Coscia, F.; Watters, K. M.; Curtis, M.; Eckert, M. A.; Chiang, C. Y.; Tyanova, S.; Montag, A.; Lastra, R. R.; Lengyel, E.; Mann, M. Integrative Proteomic Profiling of Ovarian Cancer Cell Lines Reveals Precursor Cell Associated Proteins and Functional Status. *Nat. Commun.* **2016**, *7*, 12645.

(2) Falconer, H.; Yin, L.; Grönberg, H.; Altman, D. Ovarian Cancer Risk after Salpingectomy: A Nationwide Population-Based Study. *J. Natl. Cancer Inst.* **2015**, *107* (2), dju410.

(3) Finch, A.; Shaw, P.; Rosen, B.; Murphy, J.; Narod, S. A.; Colgan, T. J. Clinical and Pathologic Findings of Prophylactic Salpingo-Oophorectomies in 159 Brca1 and Brca2 Carriers. *Gynecol. Oncol.* **2006**, *100* (1), 58−64.

(4) Klinkebiel, D.; Zhang, W.; Akers, S. N.; Odunsi, K.; Karpf, A. R. DNA Methylome Analyses Implicate Fallopian Tube Epithelia as the Origin for High-Grade Serous Ovarian Cancer. *Mol. Cancer Res.* **2016**, *14* (9), 787−794.

(5) Labidi-Galy, S. I.; Papp, E.; Hallberg, D.; Niknafs, N.; Adleff, V.; Noe, M.; Bhattacharya, R.; Novak, M.; Jones, S.; et al. High Grade Serous Ovarian Carcinomas Originate in the Fallopian Tube. *Nat. Commun.* **2017**, *8* (1), 1093.

(6) Marquez, R. T.; Baggerly, K. A.; Patterson, A. P.; Liu, J.; Broaddus, R.; Frumovitz, M.; Atkinson, E. N.; Smith, D. I.; Hartmann, L.; et al. Patterns of Gene Expression in Different Histotypes of Epithelial Ovarian Cancer Correlate with Those in Normal Fallopian Tube, Endometrium, and Colon. *Clin. Cancer Res.* **2005**, *11* (17), 6116−6126.

(7) Perets, R.; Drapkin, R. It's Totally Tubular···Riding the New Wave of Ovarian Cancer Research. *Cancer Res.* **2016**, *76* (1), 10−17.

(8) Rice, M. S.; Murphy, M. A.; Tworoger, S. S. Tubal Ligation, Hysterectomy and Ovarian Cancer: A Meta-Analysis. *J. Ovarian Res.* **2012**, *5* (1), 13.

(9) Tone, A. A.; Begley, H.; Sharma, M.; Murphy, J.; Rosen, B.; Brown, T. J.; Shaw, P. A. Gene Expression Profiles of Luteal Phase Fallopian Tube Epithelium from Brca Mutation Carriers Resemble High-Grade Serous Carcinoma. *Clin. Cancer Res.* **2008**, *14* (13), 4067−4078.

(10) Folkins, A. K.; Jarboe, E. A.; Saleemuddin, A.; Lee, Y.; Callahan, M. J.; Drapkin, R.; Garber, J. E.; Muto, M. G.; Tworoger, S.; Crum, C. P. A Candidate Precursor to Pelvic Serous Cancer (P53 Signature) and Its Prevalence in Ovaries and Fallopian Tubes from Women with Brca Mutations. *Gynecol. Oncol.* **2008**, *109* (2), 168−173.

(11) Dean, M.; Davis, D. A.; Burdette, J. E. Activin a Stimulates Migration of the Fallopian Tube Epithelium, an Origin of High-Grade Serous Ovarian Cancer, through Non-Canonical Signaling. *Cancer Lett.* **2017**, *391*, 114−124.

(12) Huang, H. S.; Hsu, C. F.; Chu, S. C.; Chen, P. C.; Ding, D. C.; Chang, M. Y.; Chu, T. Y. Haemoglobin in Pelvic Fluid Rescues Fallopian Tube Epithelial Cells from Reactive Oxygen Species Stress and Apoptosis. *Journal of pathology* **2016**, *240* (4), 484−494.

(13) King, S. M.; Hilliard, T. S.; Wu, L. Y.; Jaffe, R. C.; Fazleabas, A. T.; Burdette, J. E. The Impact of Ovulation on Fallopian Tube Epithelial Cells: Evaluating Three Hypotheses Connecting Ovulation and Serous Ovarian Cancer. *Endocr.-Relat. Cancer* **2011**, *18* (5), 627−642.

(14) Yang-Hartwich, Y.; Gurrea-Soteras, M.; Sumi, N.; Joo, W. D.; Holmberg, J. C.; Craveiro, V.; Alvero, A. B.; Mor, G. Ovulation and Extra-Ovarian Origin of Ovarian Cancer. *Sci. Rep.* **2015**, *4*, 6116.

(15) Reznik, E.; Luna, A.; Aksoy, B. A.; Liu, E. M.; La, K.; Ostrovnaya, I.; Creighton, C. J.; Hakimi, A. A.; Sander, C. A Landscape of Metabolic Variation across Tumor Types. *Cell systems* **2018**, *6* (3), 301−313.

(16) Weaver, E. M.; Hummon, A. B. Imaging Mass Spectrometry: From Tissue Sections to Cell Cultures. *Adv. Drug Delivery Rev.* **2013**, *65* (8), 1039−1055.

(17) Hoffmann, T.; Dorrestein, P. C. Homogeneous Matrix Deposition on Dried Agar for Maldi Imaging Mass Spectrometry of Microbial Cultures. *J. Am. Soc. Mass Spectrom.* **2015**, *26* (11), 1959−1962.

(18) Moree, W. J.; Phelan, V. V.; Wu, C.-H.; Bandeira, N.; Cornett, D. S.; Duggan, B. M.; Dorrestein, P. C. Interkingdom Metabolic Transformations Captured by Microbial Imaging Mass Spectrometry. *Proc. Natl. Acad. Sci. U. S. A.* **2012**, *109* (34), 13811−13816.

(19) Watrous, J. D.; Phelan, V. V.; Hsu, C.-C.; Moree, W. J.; Duggan, B. M.; Alexandrov, T.; Dorrestein, P. C. Microbial Metabolic Exchange in 3d. *ISME J.* **2013**, *7* (4), 770−780.

(20) Wiseman, J. M.; Ifa, D. R.; Song, Q.; Cooks, R. G. Tissue Imaging at Atmospheric Pressure Using Desorption Electrospray Ionization (Desi) Mass Spectrometry. *Angew. Chem., Int. Ed.* **2006**, *45* (43), 7188−7192.

(21) Yang, J. Y.; Phelan, V. V.; Simkovsky, R.; Watrous, J. D.; Trial, R. M.; Fleming, T. C.; Wenter, R.; Moore, B. S.; Golden, S. S.; et al. Primer on Agar-Based Microbial Imaging Mass Spectrometry. *J. Bacteriol.* **2012**, *194* (22), 6023−6028.

(22) Yang, Y.-L.; Xu, Y.; Straight, P.; Dorrestein, P. C. Translating Metabolic Exchange with Imaging Mass Spectrometry. *Nat. Chem. Biol.* **2009**, *5* (12), 885−887.

(23) Groseclose, M. R.; Andersson, M.; Hardesty, W. M.; Caprioli, R. M. Identification of Proteins Directly from Tissue: In Situ Tryptic Digestions Coupled with Imaging Mass Spectrometry. *J. Mass Spectrom.* **2007**, *42* (2), 254−262.

(24) Hardesty, W. M.; Caprioli, R. M. In Situ Molecular Imaging of Proteins in Tissues Using Mass Spectrometry. *Anal. Bioanal. Chem.* **2008**, *391* (3), 899−903.

(25) Norris, J. L.; Caprioli, R. M. Analysis of Tissue Specimens by Matrix-Assisted Laser Desorption/Ionization Imaging Mass Spectrometry in Biological and Clinical Research. *Chem. Rev.* **2013**, *113* (4), 2309−2342.

(26) Powers, T. W.; Neely, B. A.; Shao, Y.; Tang, H.; Troyer, D. A.; Mehta, A. S.; Haab, B. B.; Drake, R. R. Maldi Imaging Mass Spectrometry Profiling of N-Glycans in Formalin-Fixed Paraffin Embedded Clinical Tissue Blocks and Tissue Microarrays. *PLoS One* **2014**, *9* (9), e106255.

(27) Dória, M. L.; McKenzie, J. S.; Mroz, A.; Phelps, D. L.; Speller, A.; Rosini, F.; Strittmatter, N.; Golf, O.; Veselkov, K.; et al. Epithelial Ovarian Carcinoma Diagnosis by Desorption Electrospray Ionization Mass Spectrometry Imaging. *Sci. Rep.* **2016**, *6*, 39219.

(28) Sans, M.; Gharpure, K.; Tibshirani, R.; Zhang, J.; Liang, L.; Liu, J.; Young, J. H.; Dood, R. L.; Sood, A. K.; Eberlin, L. S. Metabolic Markers and Statistical Prediction of Serous Ovarian Cancer Aggressiveness by Ambient Ionization Mass Spectrometry Imaging. *Cancer Res.* **2017**, *77* (11), 2903−2913.

(29) Paine, M. R. L.; Kim, J.; Bennett, R. V.; Parry, R. M.; Gaul, D. A.; Wang, M. D.; Matzuk, M. M.; Fernández, F. M. Whole Reproductive System Non-Negative Matrix Factorization Mass Spectrometry Imaging of an Early-Stage Ovarian Cancer Mouse Model. *PLoS One* **2016**, *11* (5), e0154837.

(30) Wang, S.; Chen, X.; Luan, H.; Gao, D.; Lin, S.; Cai, Z.; Liu, J.; Liu, H.; Jiang, Y. Matrix-Assisted Laser Desorption/Ionization Mass Spectrometry Imaging of Cell Cultures for the Lipidomic Analysis of Potential Lipid Markers in Human Breast Cancer Invasion. *Rapid Commun. Mass Spectrom.* **2016**, *30* (4), 533−542.

DOI: 10.1021/acscentsci.8b00405
ACS Cent. Sci. 2018, 4, 1360−1370

(31) Li, H.; Hummon, A. B. Imaging Mass Spectrometry of Three-Dimensional Cell Culture Systems. *Anal. Chem.* **2011**, *83* (22), 8794−8801.
(32) Eddie, S. L.; Quartuccio, S. M.; Ó hAinmhir, E.; Moyle-Heyrman, G.; Lantvit, D. D.; Wei, J.-J.; Vanderhyden, B. C.; Burdette, J. E. Tumorigenesis and Peritoneal Colonization from Fallopian Tube Epithelium. *Oncotarget* **2015**, *6* (24), 20500−20512.
(33) Creedon, E.; Kowalski, J.-M.; Kowalski, P.; Kellersberger, K.; Agar, N.; Laukien, S. *Application Note # Mt-92: Vitro Mouse Tissue Imaging of an Anti-Tumor Drug, Temozolomide, with Maldi-Tof/Tof Mass Spectrometry*; Bruker Daltonics, 2008.
(34) Phelan, V. V.; Dorrestein, P. C.; Cornett, S. *Application Note FTMS-48: Microbial Imaging Mass Spectrometry with Fourier Transform Ionization Mass Spectrometry*; Bruker Daltonics, 2013.
(35) Jackson, K. S.; Inoue, K.; Davis, D. A.; Hilliard, T. S.; Burdette, J. E. Three-Dimensional Ovarian Organ Culture as a Tool to Study Normal Ovarian Surface Epithelial Wound Repair. *Endocrinology* **2009**, *150* (8), 3921−3926.
(36) King, S. M.; Modi, D. A.; Eddie, S. L.; Burdette, J. E. Insulin and Insulin-Like Growth Factor Signaling Increases Proliferation and Hyperplasia of the Ovarian Surface Epithelium and Decreases Follicular Integrity through Upregulation of the Pi3-Kinase Pathway. *J. Ovarian Res.* **2013**, *6* (1), 12.
(37) Wishart, D. S.; Jewison, T.; Guo, A. C.; Wilson, M.; Knox, C.; Liu, Y.; Djoumbou, Y.; Mandal, R.; Aziat, F.; et al. Hmdb 3.0–the Human Metabolome Database in 2013. *Nucleic Acids Res.* **2012**, *41* (D1), D801−D807.
(38) Choi, M. J.; Cho, K. H.; Lee, S.; Bae, Y. J.; Jeong, K. J.; Rha, S. Y.; Choi, E. J.; Park, J. H.; Kim, J. M.; et al. Htert Mediates Norepinephrine-Induced Slug Expression and Ovarian Cancer Aggressiveness. *Oncogene* **2015**, *34* (26), 3402−3412.
(39) Lutgendorf, S. K.; Cole, S.; Costanzo, E.; Bradley, S.; Coffin, J.; Jabbari, S.; Rainwater, K.; Ritchie, J. M.; Yang, M.; Sood, A. K. Stress-Related Mediators Stimulate Vascular Endothelial Growth Factor Secretion by Two Ovarian Cancer Cell Lines. *Clin. Cancer Res.* **2003**, *9* (12), 4514−4521.
(40) Park, S. Y.; Kang, J. H.; Jeong, K. J.; Lee, J.; Han, J. W.; Choi, W. S.; Kim, Y. K.; Kang, J.; Park, C. G.; Lee, H. Y. Norepinephrine Induces Vegf Expression and Angiogenesis by a Hypoxia-Inducible Factor-1α Protein-Dependent Mechanism. *Int. J. Cancer* **2011**, *128* (10), 2306−2316.
(41) Shahzad, M. M. K.; Arevalo, J. M.; Armaiz-Pena, G. N.; Lu, C.; Stone, R. L.; Moreno-Smith, M.; Nishimura, M.; Lee, J.-W.; Jennings, N. B.; et al. Stress Effects on Fosb- and Interleukin-8 (Il8)-Driven Ovarian Cancer Growth and Metastasis. *J. Biol. Chem.* **2010**, *285* (46), 35462−35470.
(42) Sood, A. K.; Bhatty, R.; Kamat, A. A.; Landen, C. N.; Han, L.; Thaker, P. H.; Li, Y.; Gershenson, D. M.; Lutgendorf, S.; Cole, S. W. Stress Hormone-Mediated Invasion of Ovarian Cancer Cells. *Clin. Cancer Res.* **2006**, *12* (2), 369−375.
(43) Watkins, J. L.; Thaker, P. H.; Nick, A. M.; Ramondetta, L. M.; Kumar, S.; Urbauer, D. L.; Matsuo, K.; Squires, K. C.; Coleman, R. L.; et al. Clinical Impact of Selective and Nonselective Beta-Blockers on Survival in Patients with Ovarian Cancer. *Cancer* **2015**, *121* (19), 3444−3451.
(44) Arbogast, L. A.; Garris, P. A.; Rhoades, T. A.; Ben-Jonathan, N. Changes in Ovarian Norepinephrine Synthesis Throughout the Follicular and Luteal Phases. *Biol. Reprod.* **1987**, *36* (4), 899−906.
(45) Ben-Jonathan, N.; Arbogast, L. A.; Rhoades, T. A.; Bahr, J. M. Norepinephrine in the Rat Ovary: Ontogeny and De Novo Synthesis. *Endocrinology* **1984**, *115* (4), 1426−1431.
(46) Lara, H. E.; Dorfman, M.; Venegas, M.; Luza, S. M.; Luna, S. L.; Mayerhofer, A.; Guimaraes, M. A.; Rosa E Silva, A. A. M.; Ramírez, V. D. Changes in Sympathetic Nerve Activity of the Mammalian Ovary During a Normal Estrous Cycle and in Polycystic Ovary Syndrome: Studies on Norepinephrine Release. *Microsc. Res. Tech.* **2002**, *59* (6), 495−502.
(47) Lara, H. E.; Porcile, A.; Espinoza, J.; Romero, C.; Luza, S. M.; Fuhrer, J.; Miranda, C.; Roblero, L. Release of Norepinephrine from Human Ovary: Coupling to Steroidogenic Response. *Endocr. J.* **2001**, *15* (2), 187−192.
(48) Armaiz-Pena, G. N.; Allen, J. K.; Cruz, A.; Stone, R. L.; Nick, A. M.; Lin, Y. G.; Han, L. Y.; Mangala, L. S.; Villares, G. J.; Vivas-Mejia, P.; et al. Src Activation by B-Adrenoreceptors Is a Key Switch for Tumour Metastasis. *Nat. Commun.* **2013**, *4*, 1403.
(49) Greiner, M.; Paredes, A.; Rey-Ares, V.; Saller, S.; Mayerhofer, A.; Lara, H. E. Catecholamine Uptake, Storage, and Regulated Release by Ovarian Granulosa Cells. *Endocrinology* **2008**, *149* (10), 4988−4996.
(50) Saller, S.; Merz-Lange, J.; Raffael, S.; Hecht, S.; Pavlik, R.; Thaler, C.; Berg, D.; Berg, U.; Kunz, L.; Mayerhofer, A. Norepinephrine, Active Norepinephrine Transporter, and Norepinephrine-Metabolism Are Involved in the Generation of Reactive Oxygen Species in Human Ovarian Granulosa Cells. *Endocrinology* **2012**, *153* (3), 1472−1483.
(51) Domcke, S.; Sinha, R.; Levine, D. A.; Sander, C.; Schultz, N. Evaluating Cell Lines as Tumour Models by Comparison of Genomic Profiles. *Nat. Commun.* **2013**, *4*, 2126.
(52) Bell, D.; et al. Integrated Genomic Analyses of Ovarian Carcinoma. *Nature* **2011**, *474* (7353), 609−615.
(53) Ahn, J. H.; Kim, T. J.; Lee, J. H.; Choi, J. H. Mutant P53 Stimulates Cell Invasion through an Interaction with Rad21 in Human Ovarian Cancer Cells. *Sci. Rep.* **2017**, *7* (1), 9076.
(54) Quartuccio, S. M.; Karthikeyan, S.; Eddie, S. L.; Lantvit, D. D.; Ó hAinmhire, E.; Modi, D. A.; Wei, J.-J.; Burdette, J. E. Mutant P53 Expression in Fallopian Tube Epithelium Drives Cell Migration. *Int. J. Cancer* **2015**, *137* (7), 1528−1538.
(55) Elzek, M. A.; Rodland, K. D. Proteomics of Ovarian Cancer: Functional Insights and Clinical Applications. *Cancer Metastasis Rev.* **2015**, *34* (1), 83−96.
(56) Matondo, A.; Jo, Y. H.; Shahid, M.; Choi, T. G.; Nguyen, M. N.; Nguyen, N. N. Y.; Akter, S.; Kang, I.; Ha, J.; et al. The Prognostic 97 Chemoresponse Gene Signature in Ovarian Cancer. *Sci. Rep.* **2017**, *7* (1), 9689.
(57) Reznik, E.; Luna, A.; Aksoy, B. A.; Liu, E. M.; La, K.; Ostrovnaya, I.; Creighton, C. J.; Hakimi, A. A.; Sander, C. A Landscape of Metabolic Variation across Tumor Types. *Cell systems* **2018**, *6*, 301.
(58) Nagaraja, A. S.; Dood, R. L.; Armaiz-Pena, G.; Kang, Y.; Wu, S. Y.; Allen, J. K.; Jennings, N. B.; Mangala, L. S.; Pradeep, S.; et al. Adrenergic-Mediated Increases in Inhba Drive Caf Phenotype and Collagens. *JCI insight* **2017**, *2* (16), e93076.
(59) Karthikeyan, S.; Lantvit, D. D.; Chae, D. H.; Burdette, J. E. Cadherin-6 Type 2, K-Cadherin (Cdh6) Is Regulated by Mutant P53 in the Fallopian Tube but Is Not Expressed in the Ovarian Surface. *Oncotarget* **2016**, *7* (43), 69871−69882.
(60) Karst, A. M.; Levanon, K.; Drapkin, R. Modeling High-Grade Serous Ovarian Carcinogenesis from the Fallopian Tube. *Proc. Natl. Acad. Sci. U. S. A.* **2011**, *108* (18), 7547−7552.

DOI: 10.1021/acscentsci.8b00405
ACS Cent. Sci. 2018, 4, 1360−1370